Continental Shelf Research 29 (2009) 2270–2279

Contents lists available at ScienceDirect

Continental Shelf Research

journal homepage: www.elsevier.com/locate/csr

Deriving depths of deep chlorophyll maximum and water inherent optical properties: A regional model

Peng Xiu [a,*], Yuguang Liu [a], Gang Li [b], Qing Xu [c], Haibo Zong [d], Zengrui Rong [a], Xiaobin Yin [e], Fei Chai [f]

[a] Physical Oceanography Laboratory, Ocean University of China, Qingdao, China
[b] Shenzhen Key Laboratory for Coastal and Atmospheric Research, PKU-HKUST Shenzhen-Hongkong Institution, Shenzhen, China
[c] College of Traffic, College of Ocean, Hohai University, Nanjing, China
[d] State Key Laboratory of Estuarine and Coastal Research, East China Normal University, Shanghai, China
[e] Center for Space Science and Applied Research, Chinese Academy of Science, Beijing, China
[f] School of Marine Sciences, University of Maine, Orono, ME, USA

ARTICLE INFO

Article history:
Received 2 September 2008
Received in revised form
16 August 2009
Accepted 6 September 2009
Available online 15 September 2009

Keywords:
Remote sensing
Optical properties
Deep chlorophyll maximum
Stratified waters
Reflectance inversion

ABSTRACT

The Bohai Sea is a semi-enclosed inland sea with case-2 waters near the coast. A comprehensive set of optical data was collected during three cruises in June, August, and September 2005 in the Bohai Sea. The vertical profile measurements, such as chlorophyll concentration, water turbidity, downwelling irradiance, and diffuse attenuation coefficient, showed that the Bohai Sea was vertically stratified with a relative clear upper layer superimposed on a turbid lower layer. The upper layer was found to correspond to the euphotic zone and the deep chlorophyll maximum (DCM) occurs at the base of this layer. By tuning a semi-analytical model (Lee et al., 1998, 1999) for the Bohai Sea, we developed a method to derive water inherent optical properties and the depth of DCM from above-surface measurements. Assuming a 'fake' bottom in the stratified water, this new method retrieves the 'fake' bottom depth, which is highly correlated with the DCM depth. The average relative error between derived and measured values is 33.9% for phytoplankton absorption at 440 nm, 25.6% for colored detrital matter (detritus plus gelbstoff) absorption at 440 nm, and 24.2% for the DCM depth. This modified method can retrieve water inherent optical properties and monitor the depth of DCM in the Bohai Sea, and the method is also applicable to other stratified waters.

1. Introduction

The deep chlorophyll maximum (DCM) is a widespread feature of the fresh water, the coastal zone, the shelf areas and the open oceans. Its vertical location is usually found to be near or at the base of the euphotic zone (Cullen and Eppley, 1981; Cullen, 1982). Occurrence of DCM has been explained as adaption to low light levels (Anderson, 1969), or as intrusions of nutrient rich water into the photic zone (Richardson et al., 2000). The importance of contributions of DCM to ocean color remote sensing and marine ecosystem has been extensively studied. André (1992) suggested that the influence of the vertical structure of chlorophyll on remote-sensing observations is significant when DCM is present in the upper few meters of the water column. The existence of vertical chlorophyll non-uniformity can introduce an error of about 70% to above-surface remote-sensing reflectance (Stramska and Stramski, 2005; Xiu et al., 2008). In addition, assuming a homogeneous chlorophyll profile could result in underestimating of integrated productivity by as much as 60% with respect to the value derived from the non-homogeneous profile (Hidalgo-González and Alvarez-Borrego, 2000).

In addition to the discussions over DCM generating mechanisms (e.g. Steele, 1964; Tett et al., 2002; Fennel and Boss, 2003), a large effort has been recently directed to detect DCM existence and to retrieve DCM properties using remote-sensing method. Millán-Núñez et al. (1997) developed empirical relationships to estimate the depth and the concentration of DCM in the California Current System. Silulwane et al. (2002) used a neural network to characterize and parameterize the shape of chlorophyll profiles. Uitz et al. (2006) examined the potential of using near-surface chlorophyll concentration to estimate vertical phytoplankton distribution. While most of these studies mainly focus on the open ocean where colored dissolved organic matter (CDOM) and suspended particulate matter (SPM) do not influence light penetration significantly, whether we can estimate DCM properties in coastal regions and how to do that using remote-sensing method are still not well developed.

Lee et al. (1998, 1999) developed an optimization technique that simultaneously derives water optical properties and water bottom depths by inverting a semi-analytical reflectance model and optimizing its unknown parameters. Different from other

* Corresponding author. Present address: School of Marine Sciences, University of Maine, Orono, Maine, USA.
E-mail address: pengxiucn@gmail.com (P. Xiu).

0278-4343/$ - see front matter © 2009 Elsevier Ltd. All rights reserved.
doi:10.1016/j.csr.2009.09.003

empirical models (Holden and LeDrew, 2000; Anstee et al., 2001; D'Alimonte et al., 2004), Lee's method assumes the spectral shape of bottom albedo and allows the change of albedo intensity. These methods have been used to estimate optical properties in different water bodies ranging from open oceans to coastal regions (Albert and Mobley, 2003), and derive ocean bottom properties (Goodman, 2004). In this study, we provide an alternative method to estimate water inherent optical properties and DCM properties in a coastal region of the Bohai Sea using Lee's model that was locally tuned with measured data. Here, DCM properties are focused on the vertical depths of DCM, as previous work has already been done to derive the concentration of chlorophyll in the DCM from remote-sensing data in this region (Xiu et al., 2007).

2. Data and methods

2.1. Data measurements

The Bohai Sea of China is a semi-enclosed inland sea with case-2 waters located at the northernmost end of eastern Chinese mainland between 37°07′–41°N and 117°35′–122°15′E. It is a shallow sea with a maximum depth of 85 m (in the Bohai Strait), an average depth of 18 m and half of the sea area is shallower than 20 m (Liu and Zhang, 2000). According to the geographical locations, the coastal region is divided into four areas: HHK, BHW, QHD, and LDW. Fig. 1 shows the four areas and station locations sampled in three cruises during June, August and September in 2005. The data obtained in these areas were randomly grouped into two parts: The first part with about 70% of the total numbers (n=31) was used to build and tune the regional model and the second part (n=13) was used to test model performance.

Above-surface remote-sensing reflectance (R_{rs}, see Table 1 for symbols), which is defined as the ratio of the water-leaving radiance (L_w) to the downwelling irradiance (E_d) just above the sea surface, was determined according to the method of above-water measurement protocol (Lee et al., 1996; Lee and Carder, 2004) using ASD (Analytical Spectral Devices, Inc.), a spectral radiometer with 701 spectral bands covering a wavelength range from 350 to 1050 nm.

Vertical profiles of total attenuation without water contribution, $c(\lambda,z)$, and absorption, $a(\lambda,z)$, were measured at nine wavelengths

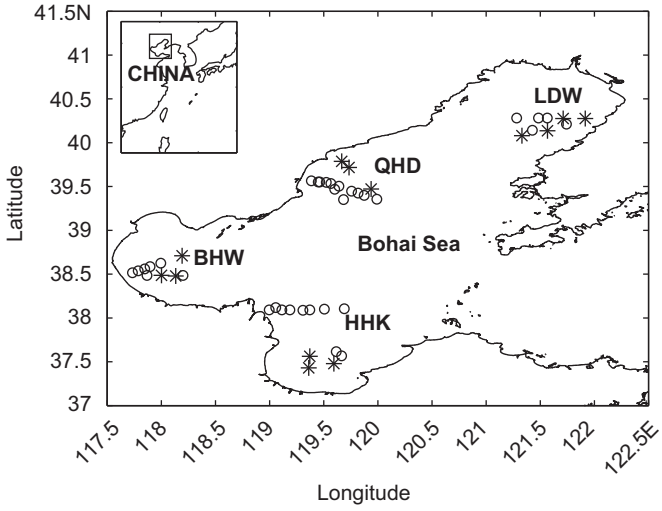

Fig. 1. Map of the Bohai Sea of China, showing major geographical features and the sampling stations in this study. The circles denote locations of part 1 data that is used to tune the regional model, and the stars denote locations of part 2 data that is used to test the model performance.

Table 1
Parameters and symbols.

a_w	Absorption coefficient of pure water	m^{-1}
a_φ	Absorption coefficient of phytoplankton	m^{-1}
a_g	Absorption coefficient of CDOM	m^{-1}
a_d	Absorption coefficient of detritus	m^{-1}
a_p	Absorption coefficient of particles ($=a_d+a_\varphi$)	m^{-1}
a	Absorption coefficient without seawater ($=a_d+a_\varphi+a_g$)	m^{-1}
a_{tot}	Total absorption coefficient ($=a_d+a_\varphi+a_g+a_w$)	m^{-1}
a_{cdm}	Absorption coefficient of detritus and CDOM ($=a_d+a_g$)	m^{-1}
b_b	Backscattering coefficients	m^{-1}
b_{bw}	Backscattering coefficients of pure water	m^{-1}
b_p	Scattering coefficients of suspended particles	m^{-1}
b_{bp}	Backscattering coefficients of suspended particles	m^{-1}
c	Attenuation coefficients without seawater	m^{-1}
chl	Chlorophyll-a concentration	mg/m^3
E_d	Downwelling irradiance	$W/nm/m^2$
L_w	Water-leaving radiance	$W/m^2/nm/sr$
L_u	Upwelling radiance	$W/m^2/nm/sr$
R_{rs}	Above-surface remote-sensing reflectance	sr^{-1}
R_{rs}^{raw}	Measured above-surface remote-sensing reflectance	sr^{-1}
R_{rs}^{mod}	Modeled above-surface remote-sensing reflectance	sr^{-1}
k_d	Downwelling irradiance attenuation coefficient	m^{-1}
k_u	Upwelling radiance attenuation coefficient	m^{-1}
λ	Wavelength	nm
χ	Reflectance ratio	
r_{rs}	Subsurface remote-sensing reflectance	sr^{-1}
r_{rs}^B	Subsurface remote-sensing reflectance from bottom reflection	sr^{-1}
r_{rs}^C	Subsurface remote-sensing reflectance from water-column scattering	sr^{-1}
r_{rs}^{dp}	Subsurface remote-sensing reflectance for optically deep waters	sr^{-1}
θ	Viewing angle	rad
β	Total volume scattering coefficient	m^{-1}
α_1	Empirical coefficients for phytoplankton absorption	
α_2	Empirical coefficients for phytoplankton absorption	
θ_w	Subsurface solar zenith angle	rad
ρ	Bottom albedo spectra	
u	Function of absorption, a, and backscattering coefficient, b_b	
D_u^C	Optical path-elongation factor for water column	
D_u^B	Optical path-elongation factor for water bottom	
κ	Sum of the absorption and backscattering coefficients	m^{-1}
S	Spectral slope parameter for CDOM absorption spectra	nm^{-1}
M	Background constant for CDOM absorption spectra	m^{-1}
P	Absorption coefficient of phytoplankton at 440 nm	m^{-1}
G	Absorption coefficient of CDOM and detritus at 440 nm	m^{-1}
X	Backscattering coefficients of suspended particles at 532 nm	m^{-1}
B	Bottom albedo at 550 nm	
H	Water depth	m
E	Spectrally constant offset	sr^{-1}
Y	Spectral dependence of particulate backscattering	

(412–715 nm) using a WET Labs (Oregon, USA) ac-9. Measurements were corrected for the temperature and salinity dependence of absorption by pure water (Pegau et al., 1997). The non-water absorption measured by ac-9 was corrected for scattering errors using the second method of Zaneveld et al. (1994). Particulate scattering coefficient, $b_p(\lambda,z)$, was estimated as the difference between $c(\lambda,z)$ and $a(\lambda,z)$. Backscattering coefficient, $b_b(\lambda,z)$, was measured with a HydroScat-6 backscattering meter (HOBI Labs, Washington, USA) at six wavelengths: 442, 488, 532, 589, 676, and 852 nm. Underwater optical profiles of upwelling radiance, $L_u(\lambda,z)$, and downwelling irradiance, $E_d(\lambda,z)$, were measured by Profiler-II, a hyper-spectral profiler instrument made by Satlantic Inc. (Nova Scotia, Canada). With measured $E_d(\lambda,z)$ and $L_u(\lambda,z)$, profiles of $k_d(\lambda,z)$ (downwelling irradiance attenuation coefficient) and $k_u(\lambda,z)$ (upwelling radiance attenuation coefficient) were then calculated (Werdell and Bailey, 2005). Vertical profiles of in vivo chlorophyll fluorescence were measured using a fluorometer attached on a

multi-sensor logger (ALEC Electronics Ltd., Japan). All these data in vertical profiles were finally binned and smoothed into 0.3-m depth intervals using median in order to construct the data set.

Surface water samples were collected using Niskin bottles and filtered immediately. Absorption spectra due to particulates, $a_p(\lambda)$, and detritus, $a_d(\lambda)$, were determined using the quantitative filter technique with the pathlength amplification factor of 6 as suggested by Kiefer and SooHoo (1982). Absorption coefficients at 750 nm were set equal to zero as the spectra baseline. Pigments were extracted with hot methanol from which chlorophyll concentrations were determined fluorometrically (Holm-Hansen and Riemann, 1978). Phytoplankton absorption spectra, $a_\varphi(\lambda)$, were then calculated as the difference between $a_p(\lambda)$ and $a_d(\lambda)$. The CDOM absorption spectra, $a_g(\lambda)$, were measured on 0.2 μm filtered surface seawater samples using a spectrophotometer (Mueller and Fargion, 2002).

In this study, the depth of DCM was determined by using measured ac-9 absorption data. A variable, the difference between $a(676)$ and $a(650)$ from ac-9 measurements, $a(676)$–$a(650)$, often can be used to indicate the absorption due to phytoplankton chlorophyll (Davis et al., 1997; Chang and Dickey, 2001; Fennel and Boss, 2003; Sullivan et al., 2005), where $a(676)$ is the absorption coefficient at 676 nm measured by ac-9 without water absorption, and $a(650)$ is that at 650 nm. The reason for this relationship is primarily because there is a pronounced absorption peak at 676 nm for chlorophyll, while other non-water constituents do not absorb significantly. The difference, $a(676)$–$a(650)$, thus can be referred as 'red peak height', where $a(650)$ is used as the baseline. This chlorophyll absorption expression not only eliminates the effect of other absorption components in the water like CDOM and particulate matters, but also does not suffer from non-photochemical quenching like fluorometric methods (Cullen and Eppley, 1981; Cullen, 1982; Cullen and Lewis, 1995; Holm-Hansen et al., 2000). Therefore, the depth where vertical $a(676)$–$a(650)$ maximum exists was used to represent the depth of DCM in this study.

2.2. Numerical model

The numerical model used in this study is a regionally tuned version of Lee's semi-analytical model (Lee et al., 1999). By assuming the spectral shape of bottom albedo, phytoplankton absorption spectrum, CDOM absorption spectrum, and particulate backscattering spectrum, this model has been used to estimate optical properties in different water bodies ranging from open oceans to coastal regions (Albert and Mobley, 2003), and derive ocean bottom properties (Goodman, 2004). Here is a brief description of Lee's model. Remote-sensing reflectance below the sea surface is related to the remote-sensing reflectance above the sea surface, R_{rs}, by

$$R_{rs} = \frac{0.5 r_{rs}}{1 - 1.5 r_{rs}} \tag{1}$$

where r_{rs} is the subsurface remote-sensing reflectance, which can be expressed by (Maritorena et al., 1994; Lee et al., 1999)

$$r_{rs} = r_{rs}^C + r_{rs}^B \approx r_{rs}^{dp}\left\{1 - \exp\left[-\left(\frac{1}{\cos(\theta_\omega)} + \frac{D_u^C}{\cos(\theta)}\right)\kappa H\right]\right\} + \frac{1}{\pi}\rho \exp\left[-\left(\frac{1}{\cos(\theta_\omega)} + \frac{D_u^B}{\cos(\theta)}\right)\kappa H\right] \tag{2}$$

The superscripts C and B stand for column and bottom. The first term corresponds to the photons that have never interacted with the bottom, whereas those that have interacted with bottom at least once form the second term. H is the water depth, ρ is the bottom albedo spectra, θ is the viewing angle, θ_ω is the subsurface solar zenith angle and κ is equal to the sum of the absorption and backscattering coefficients. r_{rs}^{dp} is the subsurface remote-sensing reflectance for optically deep waters

$$r_{rs}^{dp} \approx (0.084 + 0.170u)u \tag{3}$$

where u is calculated by

$$u = \frac{b_b}{a_{tot} + b_b} \tag{4}$$

The optical path-elongation factors for the water column, D_u^C, and water bottom, D_u^B, are

$$D_u^C \approx 1.03(1 + 2.4u)^{0.5} \tag{5}$$

$$D_u^B \approx 1.04(1 + 5.4u)^{0.5} \tag{6}$$

where

$$a_{tot} = a_w + a_\varphi + a_{cdm} \tag{7}$$

$$b_b = b_{bw} + b_{bp} \tag{8}$$

where absorption due to water, a_w are taken from Pope and Fry (1997), and backscattering due to water, b_{bw} are taken from Morel (1974). a_φ is the phytoplankton absorption coefficient, a_{cdm} is the CDM absorption due to the contribution of both detritus and CDOM, and b_{bp} is the particulate backscattering coefficient.

3. Results and discussions

3.1. Bio-optical properties in the Bohai Sea

As shown in Fig. 2, the mean spectra of $R_{rs}(\lambda)$ for HHK and BHW are similar in shape, with maximum at wavelengths of 570–580 nm, and those for QHD and LDW are similar in shape, with maximum at wavelengths of 560–570 nm. $R_{rs}(\lambda)$ spectra at green wavelengths for HHK and BHW are approximately 3-fold higher than those for QHD and LDW, indicating an increase in backscattering relative to absorption.

Absorption coefficient, $a(443)$, estimated as the sum of $a_d(443)$, $a_g(443)$ and $a_\varphi(443)$, ranges between 0.5 and 0.9 m^{-1} (Table 2). CDOM absorption, $a_g(443)$, generally dominates the absorption field, accounting for 76% of the total absorption, which is much higher than phytoplankton contribution. Higher detritus absorption, $a_d(443)$ of about 0.17 m^{-1} in HHK and BHW compared to 0.09 m^{-1} in LDW and QHD reflects the influence of the discharge of some large rivers, such as Yellow River and Haihe River on the bio-optical properties in these areas.

Based on simultaneous measurements of $b_b(442)$ and $b_p(440)$ from HS-6 and ac-9, a linear relationship with a calculated correlation coefficient of 0.92 between these two variables was obtained (Fig. 3). According to this figure, all measurements with values of $b_p(440)$ higher than 5.0 m^{-1} were found in HHK and BHW areas, where $b_b(442)$ ranges from 0.12 to 0.28 m^{-1} indicating higher concentrations of particulate matter compared with LDW and QHD areas. The slope derived from linear regression analysis, 0.032, is a little higher than 0.018 obtained by Gould et al. (1999) and 0.021 provided by Morel (1988), reflecting the more important role of the backscattering to scattering in the Bohai Sea, which might be related to the different size distributions of particles among these studies (Loisel et al., 2007).

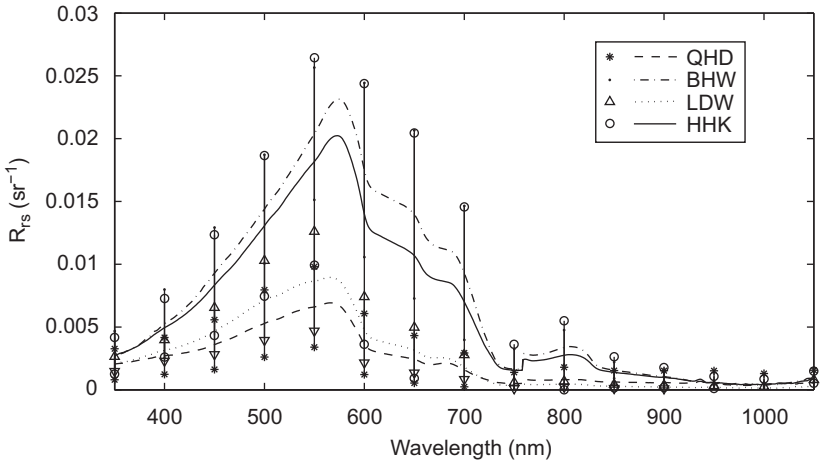

Fig. 2. Mean above-surface remote-sensing reflectance spectra, R_{rs}, measured in QHD, BHW, LDW, and HHK. The error bars represent standard deviations. Note that, these are hyperspectral data, and error bars are only plotted at every 50 nm.

Table 2
Regional mean for $a_\varphi(443)$ (m^{-1}), $a_d(443)$ (m^{-1}), $a_g(443)$ (m^{-1}) and $b_b(443)$ (m^{-1}), at the four areas, HHK, BHW, QHD, and LDW.

BHW	HHK	LDW	QHD
a_φ=0.025	a_φ=0.042	a_φ=0.058	A_φ=0.031
a_d=0.156	a_d=0.194	a_d=0.096	a_d=0.088
a_g=0.697	a_g=0.568	a_g=0.481	a_g=0.410
b_b=0.304	b_b=0.222	b_b=0.046	b_b=0.032

Previous study has shown that vertical stratification is a common feature in the Bohai Sea (Xiu et al., 2007). In this stratified water, the whole water column can be divided into two layers. The lower layer often contains high concentrations of inorganic suspended matter, which are transported by some large rivers such as Yellow River, Liaohe River and Haihe River. Fig. 4 shows vertical profiles of different variables measured in a HHK station at 38.1N, 119.5E. Temperature profile clearly indicates the existence of two layers (at about 6 m depth): in the upper layer, the temperature decreases from 25.7 °C at surface to about 24.8 °C at 6 m, while in the lower layer, the temperature remains relatively constant below 6 m. Total volume scattering coefficient $\beta(117^\circ, 470)$ is below 0.005 m^{-1} in the upper 7 m layer indicating a clear upper layer compared to the lower layer. However, the figure shows that the transition layer begins at 6 m because $\beta(117^\circ, 470)$ remains constant in the upper 6 m. Stratification is also found from measured diffuse attenuation coefficient ($k_d(490)$), which exhibits a constant value of about 0.23 m^{-1} in the upper layer, and a rapid increase from 0.25 at 6 m to 0.8 m^{-1} at 16 m. Considering the optical processes in this situation theoretically, light photons can penetrate the upper layer without suffering strong attenuation. When reaching the interface (the base of thermocline) between the upper and lower layers, most of the light photons are backscattered instead of entering the lower layer because of the high concentrations of suspended matter within it. To simplify this optical process, we consider the mechanism of light penetration in this situation is similar to what happens in clear waters with detectable bottom.

DCMs are usually present at the base of the euphotic zone where it is easier for phytoplankton to get both light and nutrient supply. In stratified waters, the depth of the euphotic zone is thought to be coincident with (or less than) the depth of the upper layer, because light cannot enter the lower layer. Fig. 5 shows a statistical relationship between measured DCM depths and the base of thermocline depths (the same as interface between upper and lower layer). This implies that the base of thermocline depth can be used as a good indicator of the DCM depth.

3.2. Model implementation

Based on these properties and previous studies which show that DCM is detectable from remote-sensing method during summer in the Bohai Sea (Xiu et al., 2007), we first hypothesize that the base of thermocline depth could be treated as a 'fake' ocean bottom, at which light cannot go through but can only reflect. Once we retrieved the 'fake' bottom depths, DCM depths are then obtained accordingly. The numerical model is based on Lee's method. Measurement data shows that, suspended matter in Bohai Sea is largely composed of sand (Xiu et al., 2007). Therefore, to derive the 'fake' bottom depths, sand albedo is used here

$$\rho(\lambda) = B\rho_{sand}(\lambda) \tag{9}$$

where B is the bottom albedo intensity at 550 nm, $\rho_{sand}(\lambda)$ is the standard 550-nm-normalized spectrum (see Fig. 2 in Lee et al., 1999). This expression allows bottom albedo spectrum to vary only in magnitude but not in spectrum shape.

In order to apply Lee's method to our study area, first we parameterize the model using the regionally measured data. The three spectrum models that need to be tuned are phytoplankton absorption, CDM absorption, and particulate backscattering. The data used to tune the model comes from our first part of the data set (n=31), and part 2 data is only used to test the model.

A single-parameter model to simulate the phytoplankton absorption spectrum, a_φ, is used here

$$a_\varphi(\lambda) = [\alpha_1(\lambda) + \alpha_2(\lambda)\ln(P)]P \tag{10}$$

where P=$a_\varphi(440)$ (unit: m^{-1}) is the phytoplankton absorption coefficient at 440 nm, $\alpha_1(\lambda)$ and $\alpha_2(\lambda)$ are the empirical coefficients. Using this expression, the number of unknowns related to $a_\varphi(\lambda)$ is reduced to one. For each sampling station, a non-linear fit technique using iterative method (Lagarias et al., 1998), was applied to Eq. (10) with measured $a_\varphi(\lambda)$ to get one pair of $\alpha_1(\lambda)$ and $\alpha_2(\lambda)$. Then spatially averaged values were chosen to tune the model. Density scatter plot shows a good agreement between measured and modeled $a_\varphi(\lambda)$ for the whole visible spectrum (ranging from 400 to 700 nm) and all of the part 1 data set (Fig. 6). For the spectrum comparison, Fig. 7 shows four example stations

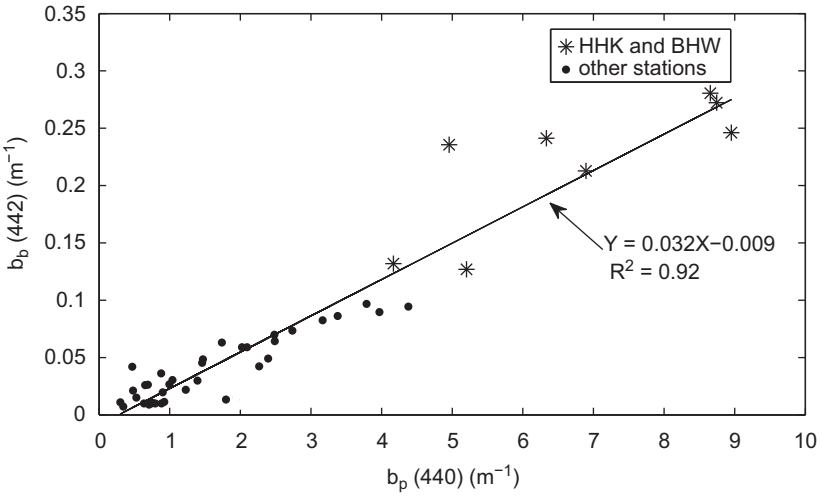

Fig. 3. Backscattering coefficient, $b_b(442)$, plotted as a function of particulate scattering coefficient $b_p(440)$ for both part 1 and part 2 data sets. The solid line represents the least-square regression fit to the data. Stars denote those data measured in HHK and BHW, and dots denote the rest.

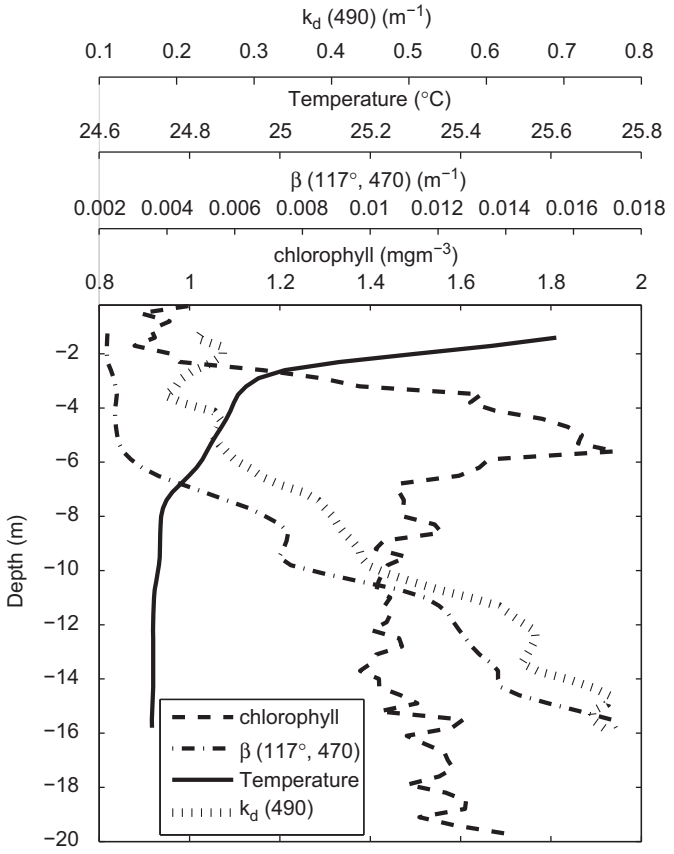

Fig. 4. Vertical distributions of diffuse attenuation coefficient ($k_d(490)$), temperature, chlorophyll concentration measured by fluorometer, and total volume scattering coefficient ($\beta(117^\circ,470)$) for a station at 38.1N, 119.5E, as an example.

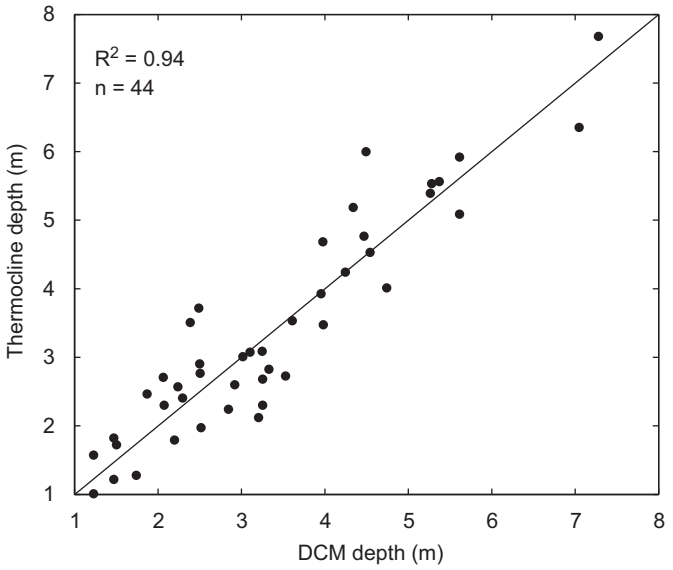

Fig. 5. Scatter plot of measured DCM depths and the base of thermocline depths (the interface between the upper layer and the lower layer). The solid line in the figure is 1:1 line.

in the four regions, where results from Lee's original $\alpha_1(\lambda)$ and $\alpha_2(\lambda)$ are also given. The mean normalized root mean square (RMS) error between the modeled and the measured a_φ of the whole visible spectrum is 0.21 for Lee's result and 0.13 for this study. The mean normalized bias (MNB) (systematic error) is 0.28 for Lee's result and 0.16 for this study.

CDOM and detritus both absorb strongly in the blue, exponentially decreasing with increasing wavelength, thus, inverse methods for quantifying ocean color spectra cannot differentiate between these two signals (Carder et al., 1991). We used the combined absorption of CDOM and detritus, defined as the colored detrital material (CDM) absorption coefficient, $a_{cdm}(\lambda)=a_g(\lambda)+a_d(\lambda)$, expressed by

$$a_{cdm}(\lambda) = Ge^{-S(\lambda-440)} + M \tag{11}$$

where $G=a_{cdm}(440)$ (unit: m^{-1}) denotes the CDM absorption at 440 nm, M (unit: m^{-1}) is a background constant allowing for any baseline shifts or attenuation not due to CDM (Stedmon et al., 2000; Stedmon and Markager, 2003). Variations in exponent S (unit: nm^{-1}) are thought to represent changes in the composition of the CDOM pool (Carder et al., 1989), and several processes such as photochemical reactions, biological degradation, PH fluctuations and

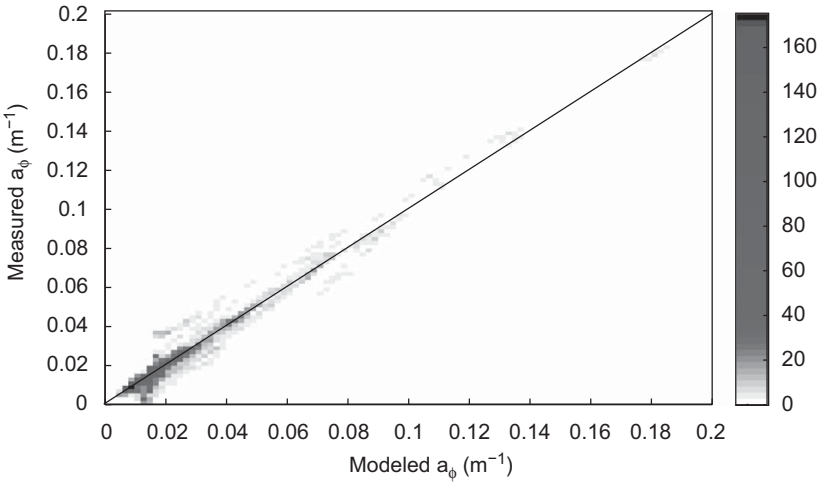

Fig. 6. Comparison of simulated phytoplankton absorption, $a_\varphi(\lambda)$, with in-situ measurements. The density scatter is plotted for the whole visible spectrum and all of the part 1 data set. Thus, the total number of points in this density plot is 301 (the number of wavelengths ranging from 400 to 700 nm with 1 nm interval) times 31 (the number of part 1 data set), equivalent to 9331. The color bar indicates the number of points and the line is 1:1 line.

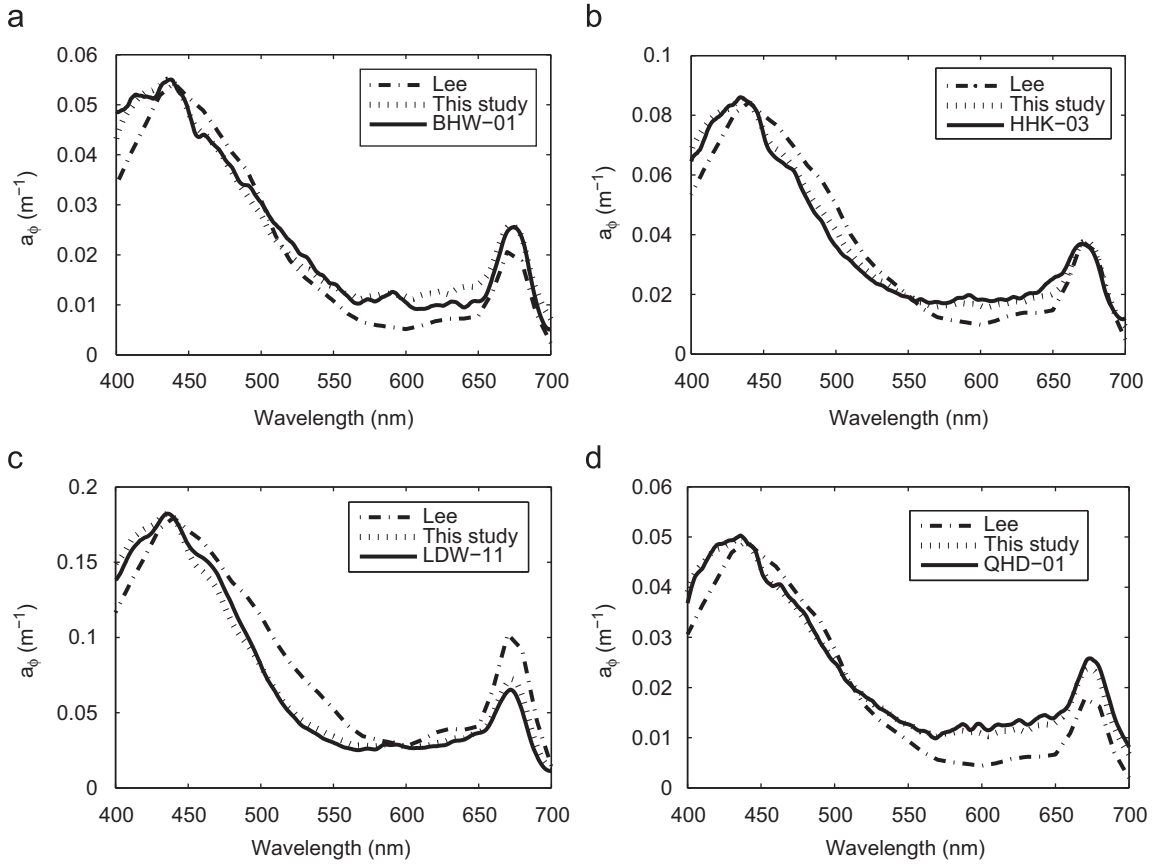

Fig. 7. Comparisons between measured and modeled phytoplankton absorption spectra, $a_\varphi(\lambda)$, in the four areas of the Bohai Sea. The solid curves denote the measured $a_\varphi(\lambda)$, dotted curves denote the results calculated by the new coefficients in this study, and dash-dotted represent those calculated from Lee's original coefficients. BHW-01, HHK-03, LDW-11 and QHD-01 are four example stations.

flocculation (Brown, 1977; Stedmon and Markager, 2003). With measured $a_{cdm}(\lambda)$ data, a non-linear fit technique using iterative method (Lagarias et al., 1998), was applied to Eq. (11). Results show that there are no significant spatial variations of values in S and M among four areas, and no significant variations are found if calculated within the UV-A and UV-B regions. Thus, spatially averaged value of 0.012 for S (ranging from 0.008 to 0.02) and 0.0035 for M (ranging from 0.0030 to 0.0037) are used in the model.

Particle backscattering spectra are modeled as

$$b_{bp}(\lambda) = X\left(\frac{532}{\lambda}\right)^{Y} \tag{12}$$

where $X = b_{bp}(532)$ (unit: m^{-1}) is the reference value, Y is a factor of spectral dependence of b_{bp}, which is sensitive to the particle size distribution. According to previous studies (Lee et al., 1999), Y

is estimated using an empirical relationship from measured $R_{rs}(440)$ and $R_{rs}(490)$ (Fig. 8).

$$Y = 1.63\chi - 2.05 \tag{13}$$

$$\chi = \exp\left(\frac{R_{rs}(440)}{R_{rs}(490)}\right) \tag{14}$$

As shown in Fig. 2, $R_{rs}(750)$ may not be zero, and it may vary from place to place. Therefore, the raw data of measured remote-sensing reflectance, $R_{rs}{}^{raw}(\lambda)$, is defined as

$$R_{rs}^{raw}(\lambda) \approx R_{rs}(\lambda) + E \tag{15}$$

where E is a spectrally constant offset serving as the spectrum error baseline. Using this expression before the measured $R_{rs}{}^{raw}(\lambda)$ is substituted into the model, we can derive the water inherent optical properties more accurately.

After tuning the model, we have six unknown parameters of P, G, X, B, H, and E from Eqs. (1)–(15). These six unknowns uniquely influence the remote-sensing reflectance. To derive these values, an optimization scheme was applied. First we set the initial values of these six unknowns using the same method as Lee et al. (1999); second, calculate a modeled value, $R_{rs}{}^{mod}(\lambda)$ from Eqs. (1)–(15) by using measured $R_{rs}{}^{raw}(\lambda)$ data; third, use a predictor–corrector scheme iteratively until the differences between $R_{rs}{}^{mod}(\lambda)$ and $R_{rs}(\lambda)$ (derived from Eq. (15)) are minimized (Lee et al., 1999), the difference is defined as

$$err = \frac{[\sum_{400}^{675}(R_{rs}^{mod} - R_{rs})^2 + \sum_{750}^{830}(R_{rs}^{mod} - R_{rs})^2]^{0.5}}{\sum_{400}^{675} R_{rs} + \sum_{750}^{830} R_{rs}} \tag{16}$$

For each set of values of the six unknowns, an optimization program computes the difference function and repeats the process with another different set until the error reaches a minimum. Then values of the six unknowns are derived. The core technique in the optimization program is the scheme of searching the minimum of error function. A Levenberg-Marquardt algorithm that seeks for a global minimum rather than local minimum in the error function was used in this study (Albert and Mobley, 2003). Note that, once the model has been locally tuned, the only input required is the measured $R_{rs}{}^{raw}(\lambda)$ data.

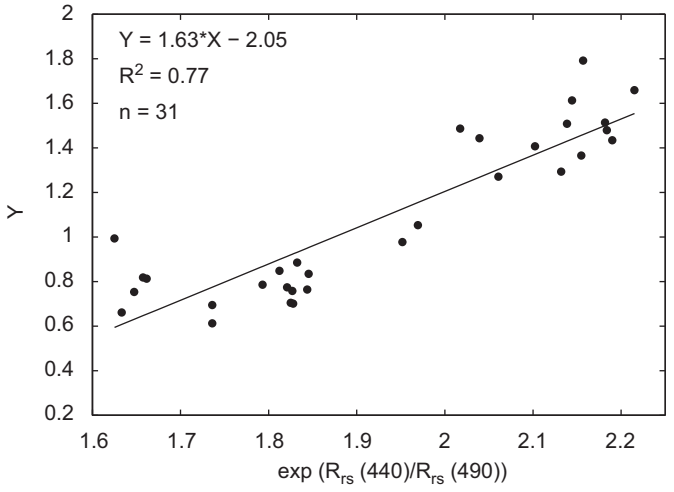

Fig. 8. For Eqs. (12)–(14), statistical relationship between spectral dependence Y and reflectance combination, $\exp(R_{rs}(440)/R_{rs}(490))$ derived based on part 1 data set.

3.3. Model results and discussion

Model performance is evaluated by applying a simple linear regression analysis of modeled values to observed P, G, and H values for both part 1 and part 2 data sets, because we do not have the in-situ measurements of X, B, and E. Comparison between modeled and measured above-surface remote-sensing reflectance for the whole visible spectrum of both part 1 and part 2 data sets suggests that this model can reasonably generate measured reflectance (Fig. 9), though sometimes the model misses the chlorophyll fluorescence due to the lack of detailed treatment of fluorescence analysis in the model (Fig. 10).

Modeled values of X and B show strong spatial variations among these four coastal areas (Fig. 11). Both X and B are found to be higher in HHK and BHW areas than in QHD and LDW areas, indicating higher scattering and stronger sand intensity in these regions. Modeled E do not show much spatial variations and its mean value for the four areas is about $-4.7\times10^{-4}\,sr^{-1}$.

Measured $a_{\varphi}(440)$ has a range of 0.006–0.26 m^{-1} and $a_{cdm}(440)$ has a range of 0.296–2.43 m^{-1} (Fig. 12(b), (d)). The value of $a_{\varphi}(440)/a_{cdm}(440)$ ranges from 0.01 to 0.33 with an average of 0.08, however, this ratio normally ranges from 1.3 to 2.5 for open ocean and from 0.13 to 0.8 for coastal waters (Lee et al., 1999; Walsh et al., 1992), which indicates that the study stations contain a wide variation of

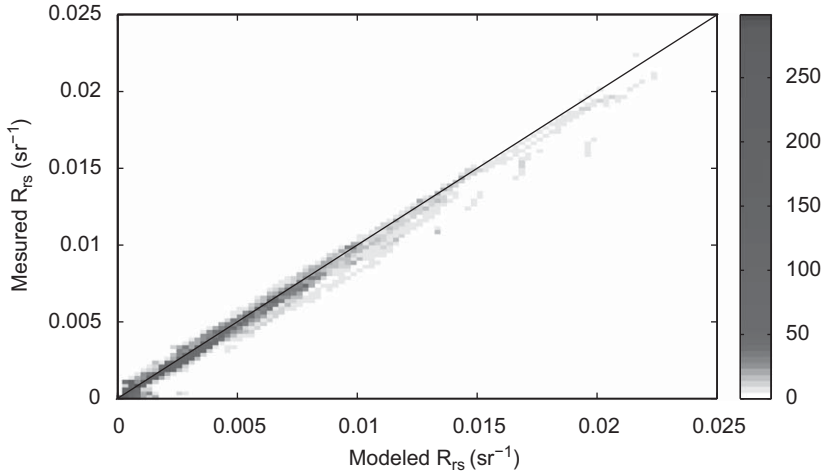

Fig. 9. Comparison between modeled and measured above-surface remote-sensing reflectance, R_{rs}, for the whole visible spectrum and all of the part 1 data set. The line in the figure is 1:1 line and the color bar indicates the number of points. The total number of points in this density plot is 401 (the number of wavelengths ranging from 400 to 800 nm with 1 nm interval) times 31 (the number of part 1 data set), equivalent to 12431.

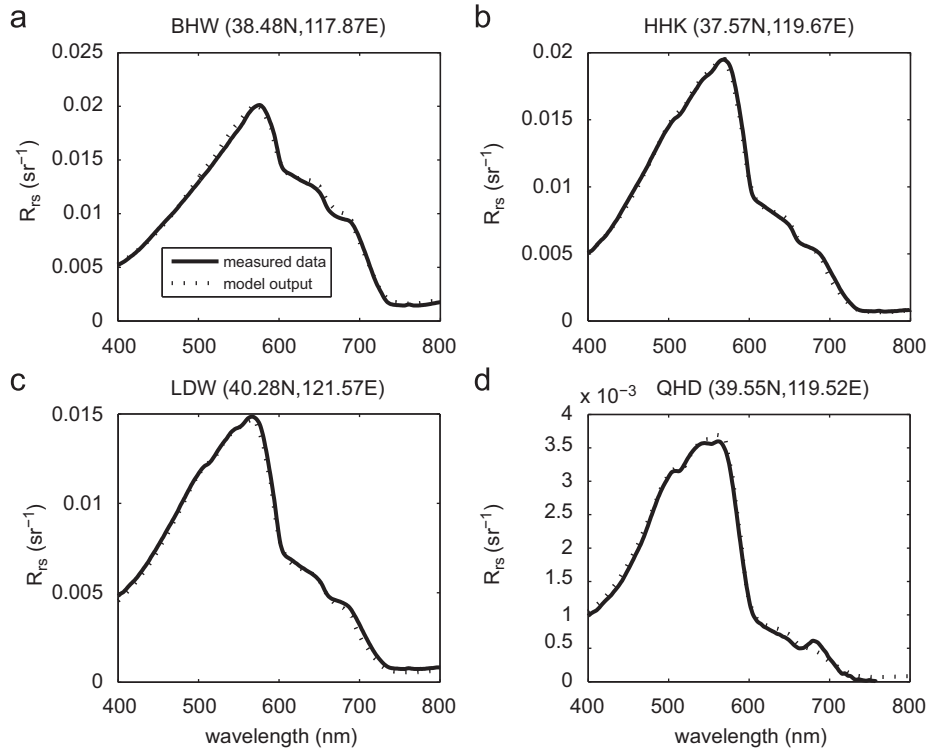

Fig. 10. Simulated above-surface remote-sensing reflectance spectra R_{rs} from a regionally tuned version of Lee's model in comparison with in-situ measurements. Solid curves denote modeled results and dotted curves denote measured ones. (a) is one example station conducted in BHW (38.48N, 117.87E), (b) is for HHK (37.57N, 119.67E), (c) is for LDW (40.28N, 121.57E), and (d) is for QHD (39.55N, 119.52E).

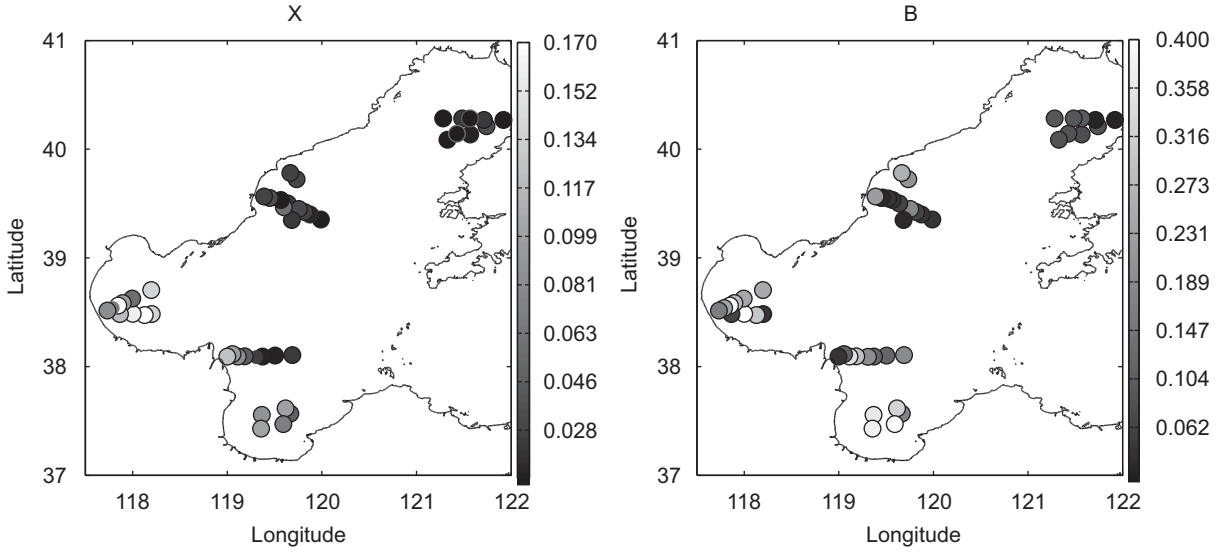

Fig. 11. Spatial distributions of modeled reference particulate backscattering coefficient, *X* (b_{bp}(532), unit: m^{-1}) and the bottom albedo intensity at 550 nm *B*. The color bar shows their values.

optical properties. For part 1 data set (n=31), the average relative error between the modeled and measured values is 42.9% for $a_{\varphi}(440)$ and 25.3% for $a_{cdm}(440)$. The RMS is 0.31 for $a_{\varphi}(440)$ and 0.14 for $a_{cdm}(440)$. The correlation coefficient between modeled and measured value is 0.88 for $a_{\varphi}(440)$ and 0.80 for $a_{cdm}(440)$. For part 2 data set (n=13), the average relative error between the model-derived and measured values is 33.9% for $a_{\varphi}(440)$ and 25.6% for $a_{cdm}(440)$. The RMS is 0.32 for $a_{\varphi}(440)$ and 0.16 for $a_{cdm}(440)$. The correlation coefficient between modeled and measured values is 0.83 for $a_{\varphi}(440)$ and 0.91 for $a_{cdm}(440)$. Overall, these results suggest that the locally tuned model performs well in retrieving water inherent optical properties considering the small values of $a_{\varphi}(440)/a_{cdm}(440)$ in case-2 waters.

Modeled depths, H, are first compared with acoustic-measured bottom depths as shown in Fig. 12(a). Clearly, model-derived depths are not the depths where ocean bottoms exist and the retrieval errors between them are relatively large (average relative error=75.9%, correlation coefficient=0.63). This verifies what we hypothesized before: Model-derived depth is not a 'real' ocean bottom depth but a 'fake' bottom depth where thermocline exists.

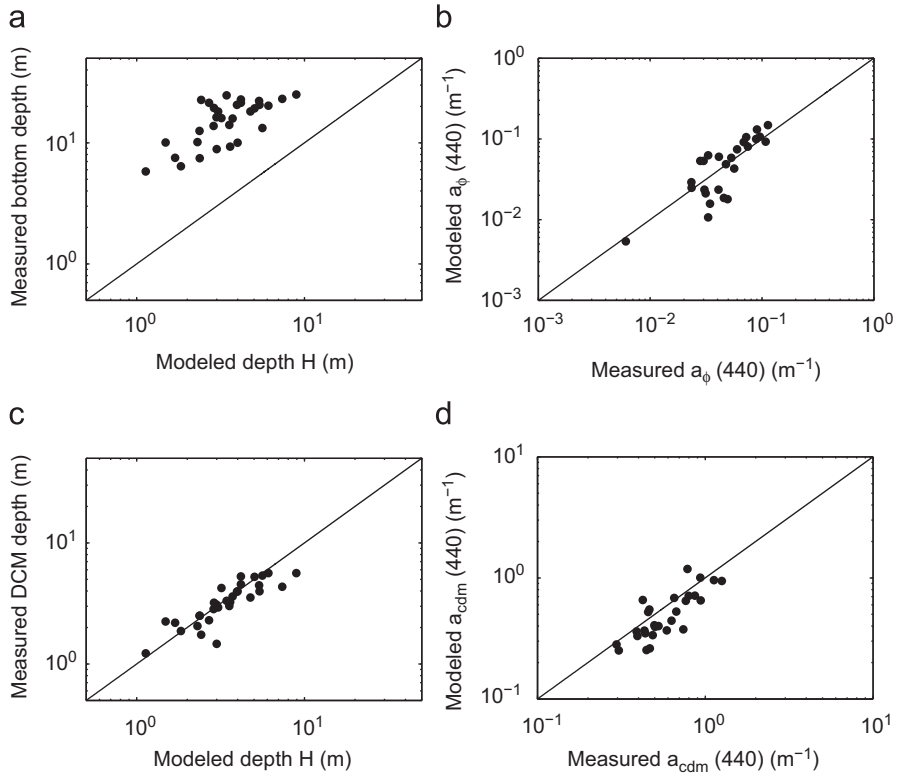

Fig. 12. Comparisons between (a) modeled depth H and measured bottom depth; (b) modeled and measured phytoplankton absorption, $a_\varphi(440)$; (c) modeled depth H and measured DCM depth; (d) modeled and measured CDM absorption, $a_{cdm}(440)$. The dots denote part 1 data set and stars denote part 2 data set.

Due to the good linear relationship between the base of thermocline depth and DCM depth in Fig. 5, modeled depths H have a robust linear correlation with DCM depths (Fig. 12(c)) for both part 1 and part 2 data sets, with average relative error = 19.2% for part 1 data and 24.4% for part 2 data, correlation coefficient = 0.83 for part 1 data and 0.88 for part 2 data.

In summary, this study demonstrates the ability of Lee's inversion method for application in the stratified Bohai Sea. The regionally tuned model is quite effective at retrieving phytoplankton and CDM absorption spectra. Lee's model was originally designed to retrieve water optical properties and bottom depths. However, after putting a 'fake' sand bottom in the coastal areas in the Bohai Sea, we find that this model also creates a method to derive the depth of the 'fake' bottom, which is consistent with the depth of DCM in stratified waters. Thus, this study provides an alternative method to retrieve DCM depths that could be further used to study the dynamics of DCM from remote-sensing data.

Acknowledgments

This work is supported by the 111 Project in China under Grant no. B07036 and State Basic Research Project under Grant no. 973-2007CB411807. We thank the editors and two anonymous reviewers for the helpful crucial reviews of the manuscript.

References

Albert, A., Mobley, C.D., 2003. An analytical model for subsurface irradiance and remote sensing reflectance in deep and shallow case-2 waters. Optics Express 11, 2873–2890.

Anderson, G.C., 1969. Subsurface chlorophyll maximum in the Northeast Pacific Ocean. Limnology and Oceanography 14, 386–391.

André, J.M., 1992. Oceanic color remote sensing and the subsurface vertical structure of phytoplankton pigments. Deep Sea Research 39, 763–779.

Anstee, J.M., Dekker, A.G., Brando, V., Pinnel, N., Byrne, G., Daniel, P., Held, A., 2001. Hyperspectral imaging for benthic species recognition in shallow coastal waters. Geoscience and Remote Sensing Symposium, 2001. IGARSS. IEEE 2001 International 6, 2513–2515.

Brown, M., 1977. Transmission spectroscopy examinations of natural waters. C. Ultraviolet spectral characteristics of the transition from terrestrial humus to marine yellow substance. Estuarine Coastal and Marine Science 5, 309–317.

Carder, K.L., Steward, R.F., Harey, R.R., Ortner, P.B., 1989. Marine humic and fulvic acids: their effects on remote sensing of ocean chlorophyll. Limnology and Oceanography 34, 68–81.

Carder, K.L., Hawes, S.K., Baker, K.A., Smith, R.C., Steward, R.G., Mitchell, B.G., 1991. Reflectance model for quantifying chlorophyll-a in the presence of productivity degradation products. Journal of Geophysical Research 96, 20599–20611.

Chang, G.C., Dickey, T.D., 2001. Optical and physical variability on time scales from minutes to the seasonal cycle on the New England shelf: July 1996–June 1997. Journal of Geophysical Research 106, 9435–9453.

Cullen, J.J., Eppley, R.W., 1981. Chlorophyll maximum layers of the Southern California Bight and possible mechanisms of their formation and maintenance. Oceanologica Acta 4 (1), 23–32.

Cullen, J.J., 1982. The deep chlorophyll maximum: comparing vertical profiles of chlorophyll a. Canadian Journal of Fisheries and Aquatic Sciences 39, 791–803.

Cullen, J.J., Lewis, M.R., 1995. Biological processes and optical measurements near the sea surface: some issues relevant to remote sensing. Journal of Geophysical Research 100, 13255–13266.

D'Alimonte, D., Zibordi, G., Berthon, J-F., 2004. Determination of CDOM and NPPM absorption coefficient spectra from coastal water remote sensing reflectance. IEEE Transactions on Geoscience and Remote Sensing 42, 1770–1777.

Davis, R.F., Moore, C.C., Zaneveld, J.R.V., Napp, J.M., 1997. Reducing the effects of fouling on chlorophyll estimates derived from long-term deployments of optical instruments. Journal of Geophysical Research 102, 5851–5855.

Fennel, K., Boss, E., 2003. Subsurface maxima of phytoplankton and chlorophyll: steady state solutions from a simple model. Limnology and Oceanography 48, 1521–1534.

Goodman, J.A., 2004. Hyperspectral remote sensing of coral reefs: deriving bathymetry, aquatic optical properties and a benthic spectral unmixing classification using AVIRIS data in the Hawaiian Islands. Ph.D. Dissertation, University of California, Davis.

Gould, R.W., Arnone, R.A., Martinolich, P.M., 1999. Spectral dependence of the scattering coefficient in case 1 and case 2 waters. Applied Optics 38, 2377–2383.

Hidalgo-González, R.M., Alvarez-Borrego, S., 2000. Chlorophyll profiles and the water column structure in the Gulf of California. Oceanologica Acta 24, 19–28.
Holden, H., LeDrew, E., 2000. Optical water column properties of a coral reef environment: towards correction of remotely sensed imagery. Geoscience and Remote Sensing Symposium, 2000. Proceedings. IGARSS 2000. IEEE 2000 International 6, 2666–2668.
Holm-Hansen, O., Riemann, B., 1978. Chlorophyll a determination: improvements in methodology. Oikos 30, 438–447.
Holm-Hansen, O., Amos, A.F., Hewes, C.D., 2000. Reliability of estimating chlorophyll a concentrations in Antarctic waters by measurement of in situ chlorophyll a fluorescence. Marine Ecology Progress Series 196, 103–110.
Kiefer, D.A., SooHoo, J.B., 1982. Spectral absorption by marine particles of coastal waters of Baja California. Limnology and Oceanography 27, 492–499.
Lagarias, J.C., Reeds, J.A., Wright, M.H., Wright, P.E., 1998. Convergence properties of the Nelder–Mead simplex method in low dimensions. SIAM Journal on Optimization 9, 112–147.
Lee, Z.P., Carder, K.L., Steward, R.G., Peacock, T.G., Davis, C.O., Mueller, J.L., 1996. Remote-sensing reflectance and inherent optical properties of oceanic waters derived from above-water measurements. Proceedings of SPIE (Ocean Optics XIII) 2963, 160–166.
Lee, Z.P., Carder, K.L., Mobley, C., Steward, R.G., Patch, J.S., 1998. Hyperspectral remote sensing for shallow waters: I. A semi-analytical model. Applied Optics 37, 6329–6338.
Lee, Z.P., Carder, K.L., Mobley, C.D., Steward, R.G., Patch, J.S., 1999. Hyperspectral remote sensing for shallow waters: 2. Deriving bottom depths and water properties by optimization. Applied Optics 38, 3831–3843.
Lee, Z.P., Carder, K.L., 2004. Absorption spectrum of phytoplankton pigments derived from hyperspectral remote-sensing reflectance. Remote Sensing of Environment 89, 361–368.
Liu, S.M., Zhang, J., 2000. Chemical oceanography of nutrient elements in the Bohai Sea, Yellow Sea and East China Sea. Marine Science Bulletin 2, 76–85 (in Chinese with English abstract).
Loisel, H., Mériaux, X., Berthon, J.-F., Poteau, A., 2007. Investigation of the optical backscattering to scattering ratio of marine particles in relation to their biogeochemical composition in the eastern English Channel and southern North Sea. Limnology and Oceanography 52, 739–752.
Maritorena, S., Morel, A., Gentili, B., 1994. Diffuse reflectance of oceanic shallow waters: influence of water depth and bottom albedo. Limnology and Oceanography 39, 1689–1703.
Millán-Núñez, R., Alvarez-Borrego, S., Trees, C.C., 1997. Modeling the vertical distribution of chlorophyll in the California Current System. Journal of Geophysical Research 102, 8587–8595.
Morel, A., 1974. Optical properties of pure water and pure sea water. In: Jerlov, N.G., Nielsen, E.S. (Eds.), Optical Aspects of Oceanography. Elsevier, New York, pp. 1–24.
Morel, A., 1988. Optical modeling of the upper ocean in relation to its biogenous matter content (case 1 waters). Journal of Geophysical Research 93, 10749–10768.
Mueller, J.L., Fargion, G.S., 2002. Ocean optics protocols for satellite ocean color sensor validation, revision 3, volume 2. NASA Technical Memorandum. 2002-210004/Rev3-Vol2, NASA Goddard Space Flight Center, Greenbelt, MD.
Pegau, W.S., Gray, D., Zaneveld, J.R.V., 1997. Absorption and attenuation of visible and near-infrared light in water: dependence on temperature and salinity. Applied Optics 36, 6035–6046.
Pope, R.M., Fry, E.S., 1997. Absorption spectrum (380–700 nm) of pure waters: II. Integrating cavity measurements. Applied Optics 36, 8710–8723.
Richardson, K., Visser, A.W., Pedersen, F.B., 2000. Subsurface phytoplankton blooms fuel pelagic production in the North Sea. Journal of Plankton Research 22, 1663–1671.
Silulwane, N.F., Richardson, A.J., Mitchell-Innes, B., Shillington, F.A., 2002. Predicting the shape of chlorophyll profiles using some novel quantitative approaches. GLOBEC Report 16, pp. 8–11.
Stedmon, C.A., Markager, S., Kaas, H., 2000. Optical properties and signatures of chromophoric dissolved organic matter (CDOM) in Danish coastal waters. Estuarine, Coastal and Shelf Science 5l, 267–278.
Stedmon, C.A., Markager, S., 2003. Behaviour of the optical properties of coloured dissolved organic matter under conservative mixing. Estuarine, Coastal and Shelf Science 57, 973–979.
Steele, J., 1964. A study of production in the Gulf of Mexico. Journal of Marine Research 3, 211–222.
Stramska, M., Stramski, D., 2005. Effects of a nonuniform vertical profile of chlorophyll concentration on remote-sensing reflectance of the ocean. Applied Optics 44, 1735–1747.
Sullivan, J.M., Twardowski, M.S., Donaghay, P.L., Freeman, S.A., 2005. Use of optical scattering to discriminate particle types in coastal waters. Applied Optics 44, 1667–1680.
Tett, P., Arístegui, J., Barton, D., Basterretxea, G., De Armas, J.D., Escánez, J.E., León, S.H., Lorenzo, L.M., Montero, N., 2002. Steady-state DCM dynamics in Canaries waters. Deep-Sea Research II 49, 3543–3559.
Uitz, J., Claustre, H., Morel, A., Hooker, S.B., 2006. Vertical distribution of phytoplankton communities in open ocean: an assessment based on surface chlorophyll. Journal of Geophysical Research 111 doi:10.1029/2005JC003207.
Walsh, J.J., Carder, K.L., Mueller-Karger, F.E., 1992. Meridional fluxes of dissolved organic matter in the North Atlantic Ocean. Journal of Geophysical Research 97, 15,625–15,637.
Werdell, P.J., Bailey, S.W., 2005. An improved in-situ bio-optical data set for ocean color algorithm development and satellite data product validation. Remote Sensing of Environment 98, 122–140.
Xiu, P., Liu, Y.G., Yin, X.B., 2007. Preliminary study on distribution of deep chlorophyll maximum and remote sensing model in the Bohai Sea of China. International Journal of Remote Sensing 28, 2599–2612.
Xiu, P., Liu, Y.G., Tang, J.W., 2008. Variations of ocean colour parameters with nonuniform vertical profiles of chlorophyll concentration. International Journal of Remote Sensing 29, 831–849.
Zaneveld, J.R.V., Kitchen, J.C., Moore, C.M., 1994. The scattering error correction of reflecting-tube absorption meters. Ocean Optics XII, Proceedings of SPIE 2258, 44–55.